



Fischer-Tropsch synthesis over methyl modified $\text{Fe}_2\text{O}_3@\text{SiO}_2$ catalysts with low CO_2 selectivity

Xufei Yu, Jianli Zhang*, Xu Wang, Qingxiang Ma, Xinhua Gao, Hongqiang Xia, Xiaoyong Lai, Subing Fan, Tian-Sheng Zhao*

State Key Laboratory of High-efficiency Utilization of Coal and Green Chemical Engineering, College of Chemistry & Chemical Engineering, Ningxia University, Yinchuan 750021, People's Republic of China



ARTICLE INFO

Keywords:

CO hydrogenation
 $\text{Fe}_2\text{O}_3@\text{SiO}_2$ catalyst
 Hydrophobic modification
 Reduced CO_2 selectivity

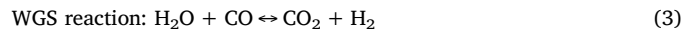
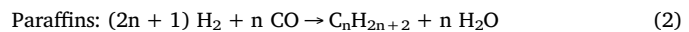
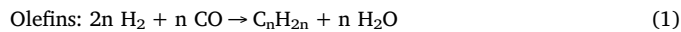
ABSTRACT

Methyl modified $\text{Fe}_2\text{O}_3@\text{SiO}_2$ catalysts with core-shell structure were fabricated through hydrothermal method, Stöber method, and following silylation reaction procedure, where the SiO_2 shell was employed as a bridge contacting Fe core and hydrophobic groups of CH_3 to obtain a highly hydrophobic surface of Fe catalyst. The synthesized catalysts showed high activity and stability toward CO hydrogenation with very low CO_2 selectivity (below 5% based on carbon) in a fixed-bed reactor. The catalyst samples were characterized by TEM, SEM, FT-IR, TG, XRD, Mössbauer spectroscopy, N_2 adsorption-desorption, H_2 -TPR, in situ CO-TPD, XPS, and water contact angle measurements. The results manifest that the hydrophobic surface by methyl modification can prevent the readsoption of water, that inhibits distinctly the water gas shift (WGS) activity and thus suppresses the production of CO_2 . Furthermore, methyl modified $\text{Fe}_2\text{O}_3@\text{SiO}_2$ catalyst exhibits higher selectivity of C_2^{\pm} - C_4^{\pm} hydrocarbons than $\text{Fe}_2\text{O}_3@\text{SiO}_2$ catalyst.

1. Introduction

Fischer-Tropsch synthesis (FTS) is a well-established process for the transformation of syngas into clean liquid fuels (gasoline, diesel fuel, and jet fuel) or valuable chemicals (olefins and aromatics), and oxygenates (methanol and C_2^+ oxygenates) [1–8]. However, the product selectivity of traditional FTS reaction usually follows the Anderson-Schulz-Flory (A-S-F) distribution [3,4], based on reaction mechanism of surface polymerization of CH_x monomers. The process economy is from time to time brought out as a result of wide product spectrum. Efficient catalysts for synthesizing desired products has been one of hotspot issues in academic community [2]. Recently, major progresses have been achieved in the development of novel catalysts or new strategies to increase selectivities of liquid fuels [4,5] and light olefins [6–9].

Iron-based catalysts are highly active for both the FTS and the water gas shift (WGS) reaction [10–12]. They can catalyze to produce more initial olefins while lower methane than other catalysts over wide ranges of reaction temperature and H_2/CO ratio [13–16], and have been extensively studied for the production of light olefins and fuels through FTS [2,3,6,15,16]. The process for hydrocarbon production over iron catalyst generally includes the following reactions:



The WGS reaction occurs alongside hydrocarbon production via the FTS reaction, two main steps involved in hydrogenation of CO . The exothermic and reversible WGS reaction is for tuning the ratio of H_2/CO and is regarded as an import side reaction in FTS [17–23], which directly affects concentrations of CO and water and exerts remarkable impact on product distribution and catalyst deactivation [23]. The high activity on the WGS reaction, however, causes to form large amounts of CO_2 [6–8]. In the case of from coal-based syngas of low H_2/CO ratio, CO_2 selectivity is even above 40% [20–22]. Therefore, suppression of CO_2 formation is of great importance in FTS. Reaction conditions (temperature, pressure, ratio of H_2/CO), catalyst factors (active components, supports, promoters) and partial pressure of water influence the WGS reaction [22–24]. Since production of CO_2 is related closely to the WGS activity, one of main pathways for CO_2 generation [24], the activity inhibition of the WGS reaction certainly will reduce the production of CO_2 (Eq. (3)). A hydrophobic surface should be favorable to inhibit the readsoption and reaction of water with CO . Chemical modification has been conducted by using different modifiers like methyl for Co-based catalyst to form a hydrophobic surface [25–28]. However, there are few reports about hydrophobic modification of iron-

* Corresponding authors.

E-mail addresses: zhangjl@nxu.edu.cn (J. Zhang), zhaots@nxu.edu.cn (T.-S. Zhao).

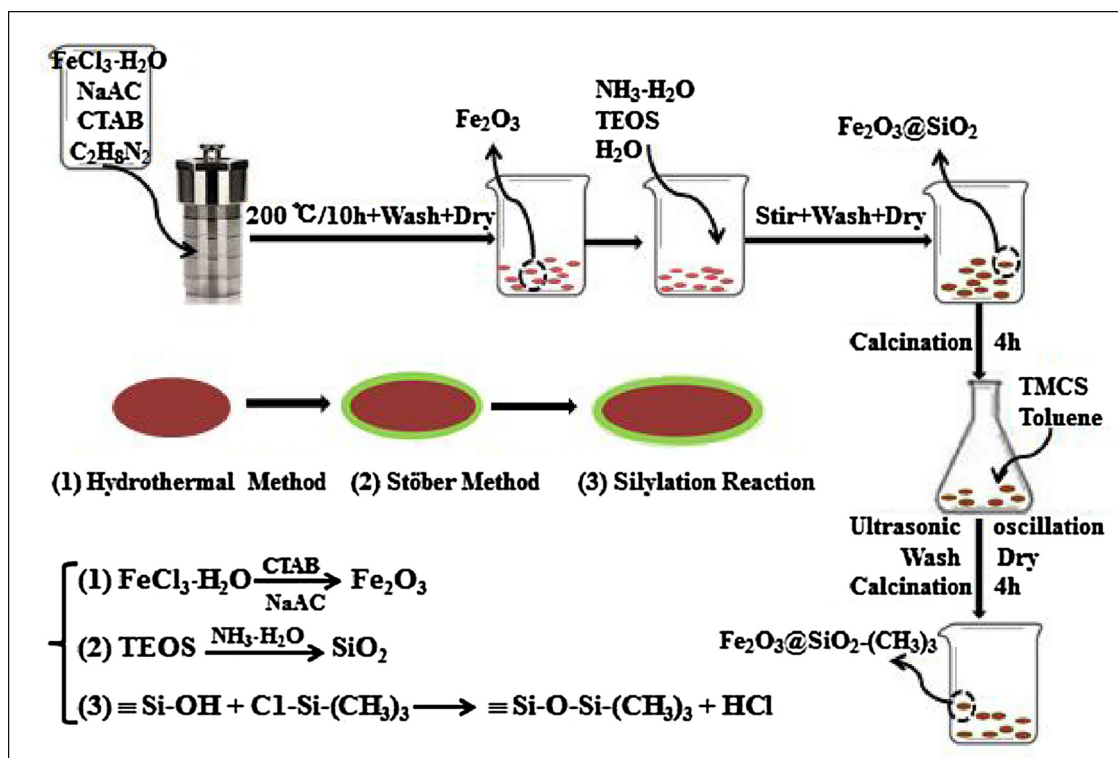


Fig. 1. Procedure for the preparation of catalyst samples.

based catalysts for FTS and effects on the WGS reactivity and hydrocarbon distribution.

Here, we report a CH₃-modified Fe₂O₃@SiO₂ core-shell structure catalyst that provides hydrophobic environment for iron active centers in the FTS reaction. With hydrophobic surface the formation of CO₂ is greatly reduced which may stem from inhibiting of the WGS activity. The selectivity of light olefins is also improved and the catalyst has good stability via this controlling of the WGS reaction.

2. Experimental

2.1. Catalyst preparation

Fe₂O₃ precursor was synthesized using a solvent thermal method [29]. Firstly, FeCl₃·H₂O (6.0 g) was dissolved in deionized water (90 mL) to form a reddish-brown solution, followed by addition of sodium acetate anhydrous (NaAC) and cetyl trimethyl ammonium bromide (CTAB), respectively. The molar ratio of FeCl₃·H₂O: NaAC: CTAB = 2.7:8.9:1. Then, 21.0 mL of ethylenediamine solution was added to the above mixed solutions under vigorous stirring to form homogeneous solution. Afterwards, the solution was transferred into a Teflon-lined stainless autoclave and heated at 200 °C for 10 h. After cooling to room temperature, a reddish-brown precursor was obtained. The resulting solid was washed repeatedly with deionized water and dried in air at 100 °C overnight. The sample was denoted as Fe₂O₃.

Fe₂O₃@SiO₂ was prepared by Stöber method as follows: Fe₂O₃ powder was dissolved in ethanol under ultrasonication to obtain a uniform suspension. The concentration of the solution is 0.0104 mol/L. Then tetraethoxysilane (TEOS) was added under magnetic stirring and the stirring continued for 3 h. Then, ammonia and deionized water were added in order under vigorous stirring for 4 h. Finally the mixed solution with a volume ratio of TEOS:NH₃·H₂O:H₂O = 1:5:20 was formed. The resulting solid was washed several times by ethanol, and then dried in air at 100 °C. The dried powder was calcined in N₂ at 350 °C for 4 h. The sample was denoted as Fe₂O₃@SiO₂.

Hydrophobically modified catalysts (Fe₂O₃@SiO₂-(CH₃)₃) were

prepared by silylation reaction as follows: Fe₂O₃@SiO₂ powder (4.0 g) was added into a conical flask. Then, 16 mL of toluene was added, and the mixture was shaken under ultrasonic waves for 5 min. Next, chlorotrimethylsilane (TMCS) was added into the conical flask, which was then treated with ultrasonic bath for 2 h at ambient temperature. The resulting product was vacuum dried at 110 °C overnight and then calcined in N₂ at 280 °C for 4 h. Different levels of silylated catalysts were obtained by varying the amount of TMCS. TMCS of 2 mL and 4 mL was employed for different samples, respectively. The obtained samples were named as A-Fe₂O₃@SiO₂-(CH₃)₃ (2 mL of TMCS) and B-Fe₂O₃@SiO₂-(CH₃)₃ (4 mL of TMCS), respectively. The whole preparation procedure is pictured in flow diagram (Fig. 1).

2.2. Catalytic characterization

The morphology of all fresh and used catalysts was characterized by KYKY-2008B scanning electron microscopy (SEM) and JEOL-JSM-7500F field transmission electron microscopy (FETEM). The catalysts were sprayed with gold at 25 kV and 3.0 kV, respectively.

BET surface area, pore volume, and pore diameter were determined on a JW-BK132F instrument by N₂ adsorption-desorption method.

Surface chemical modification of the catalysts was analyzed using FT-IR Spectroscopic (Bruker Tensor-27), which provides information of chemical bonds. Sample was mixed with KBr (mass ratio 1:200), pressed to form a disc at 10 MPa and scanned in the range of 400 cm⁻¹ to 4000 cm⁻¹.

Thermogravimetric-differential scanning calorimetry analysis was carried out on a SDT Q600 simultaneous thermal analyzer from TA instruments company (USA). Under N₂ atmosphere, the thermal stability of the catalysts was measured from room temperature to 800 °C at a heating rate of 10 °C/min.

XRD studies were performed using a Rigaku D/ MAX2200PC spectrometer at 40 kV and 30 mA using monochromatic Cu K α radiation.

The Mössbauer spectra of fresh and used catalyst samples were recorded at 298 K with a spectrometer working in the mode of constant accelerations with the use of ⁵⁷Co γ -quantum source in the Rh matrix.

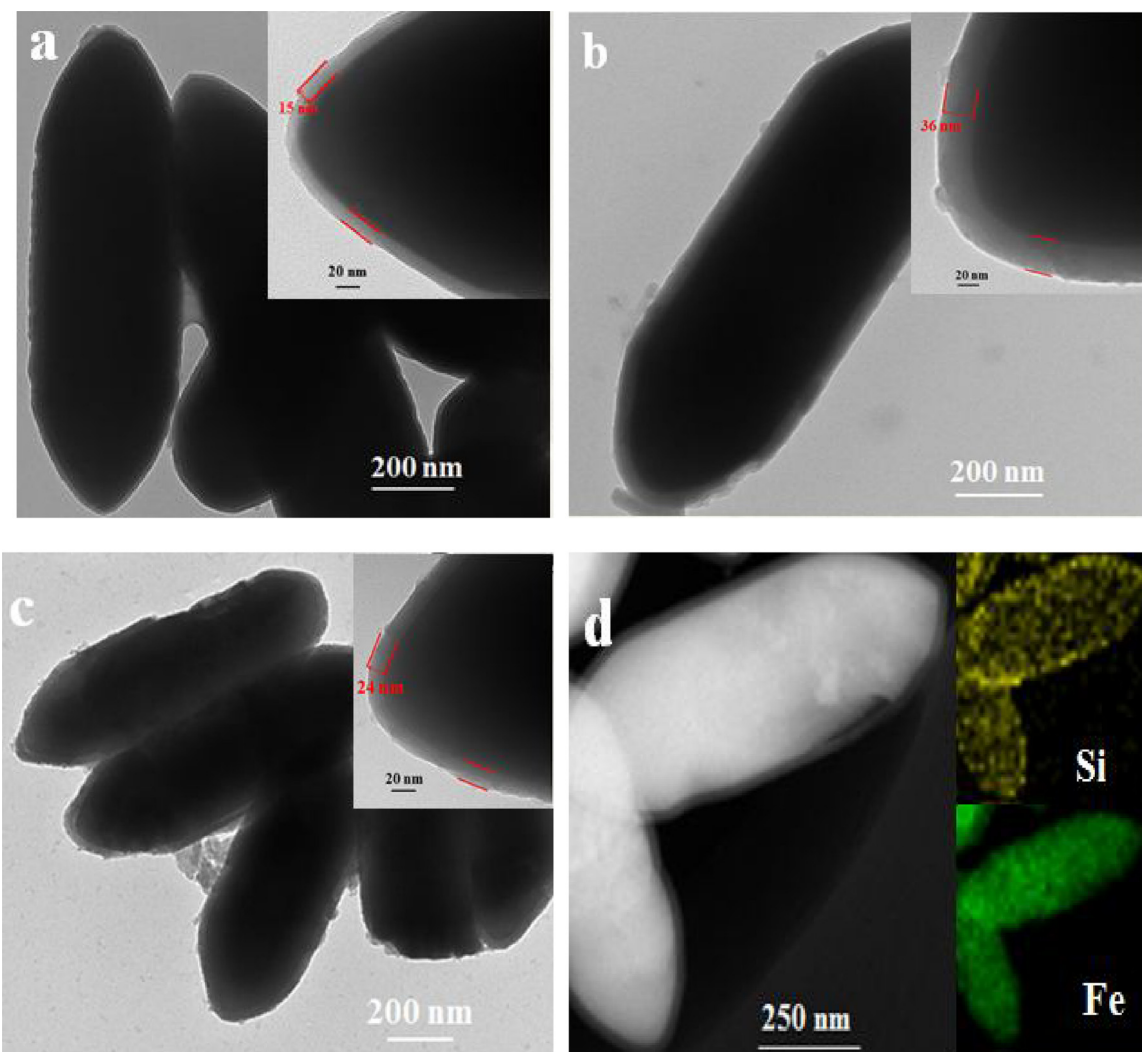


Fig. 2. TEM images of fresh catalysts for (a) $\text{Fe}_2\text{O}_3@\text{SiO}_2$, (b) $\text{A}-\text{Fe}_2\text{O}_3@\text{SiO}_2-(\text{CH}_3)_3$, (c) $\text{B}-\text{Fe}_2\text{O}_3@\text{SiO}_2-(\text{CH}_3)_3$ and (d) EDX elemental mapping of $\text{B}-\text{Fe}_2\text{O}_3@\text{SiO}_2-(\text{CH}_3)_3$.

Spectra were computer-fitted to a Lorentzian shape with a least-squares fitting procedure. The isomer shifts (IS) of the spectra were given with respect to the centroid of α -Fe at room temperature.

$\text{H}_2\text{-TPR}$ characterization of the catalysts was carried out using a TP-5080 multi-purpose adsorbent instrument. 50 mg catalyst sample was filled in a quartz tube and purged at 350 °C for 30 min in He atmosphere (30 mL/min). The temperature was reduced to room temperature and switched to a mixture gas consisting of 5% H_2 /95% N_2 (v/v) in flow of 30 mL/min. The temperature was raised at 10 °C/min to the set temperature, and the reduction curve was recorded synchronously.

Contact angle measurements were performed using the JC2000D1 contact angle goniometer at ~20 °C.

In situ CO temperature-programmed-desorption of CO (CO-TPD) was performed on an AutoChem II Chemisorption Analyzer (Micromeritics). Typically, sample of 50 mg was reduced by syngas for 4 h at 300 °C, and purged by He (30 mL min⁻¹) for 1 h. Then, the sample was cooled in a He flowing and then pulse-adsorbed by CO at 50 °C until saturation, followed by purge with He for 1 h. Desorption signal was recorded as the temperature increased from 50 °C to 800 °C at a heating rate of 10 °C/min.

X-ray photoelectron spectra (XPS) were measured on a thermo scientific ESCALAB 250 spectrometer for the whole samples with an Al K α X-ray source. The base pressure of the chamber was less than 2×10^{-8} Pa. Binding energies (BEs) were calibrated relative to adventitious carbon using the C 1s peak at 284.8 eV.

2.3. Catalytic reaction tests

FTS reaction was carried out in a stainless steel fixed-bed reactor (i.d. = 8 nm). The catalyst (1 mL) and the quartz sand (1 mL) were mechanically mixed. Prior to the FTS, the catalyst was reduced in situ at 300 °C and 0.1 MPa under syngas ($\text{H}_2/\text{CO} = 2$) flow for 4 h. The FT reaction was performed at 320 °C, 1.5 MPa, 3000 h⁻¹, and H_2/CO ratio of 2. Data were taken at the steady state after 12 h on stream. The tail gas was analyzed online by gas chromatograph (GC-9560) equipped with TCD and FID detector. Liquid products were collected in a cold trap and a hot trap respectively and then were off-line analyzed by gas chromatograph (GC-9560) equipped with a capillary column.

CO conversion and the CO_2 selectivity were calculated based on carbon basis.

$$\text{CO conv.} = (\text{F}_{\text{in}} \times y_{\text{in}}^{\text{CO}} \cdot \text{F}_{\text{out}} \times y_{\text{out}}^{\text{CO}}) / (\text{F}_{\text{in}} \times y_{\text{in}}^{\text{CO}}) \times 100 \%$$

$$\text{CO}_2 \text{ sel.} = (\text{F}_{\text{out}} \times y_{\text{out}}^{\text{CO}_2}) / (\text{F}_{\text{in}} \times y_{\text{in}}^{\text{CO}} \times \text{CO conv.}) \times 100 \%$$

where, F_{in} was the mole flow rate of the feed gas, mol h⁻¹; F_{out} was the mole flow rate of the effluent, mol h⁻¹; $y_{\text{in CO}}$ was the volume fraction of CO in the feed gas; $y_{\text{out CO}}$ was the volume fraction of CO or CO_2 in the effluent.

Calculation for hydrocarbon product selectivity was based on the weight content (wt%) of the corresponding hydrocarbons.

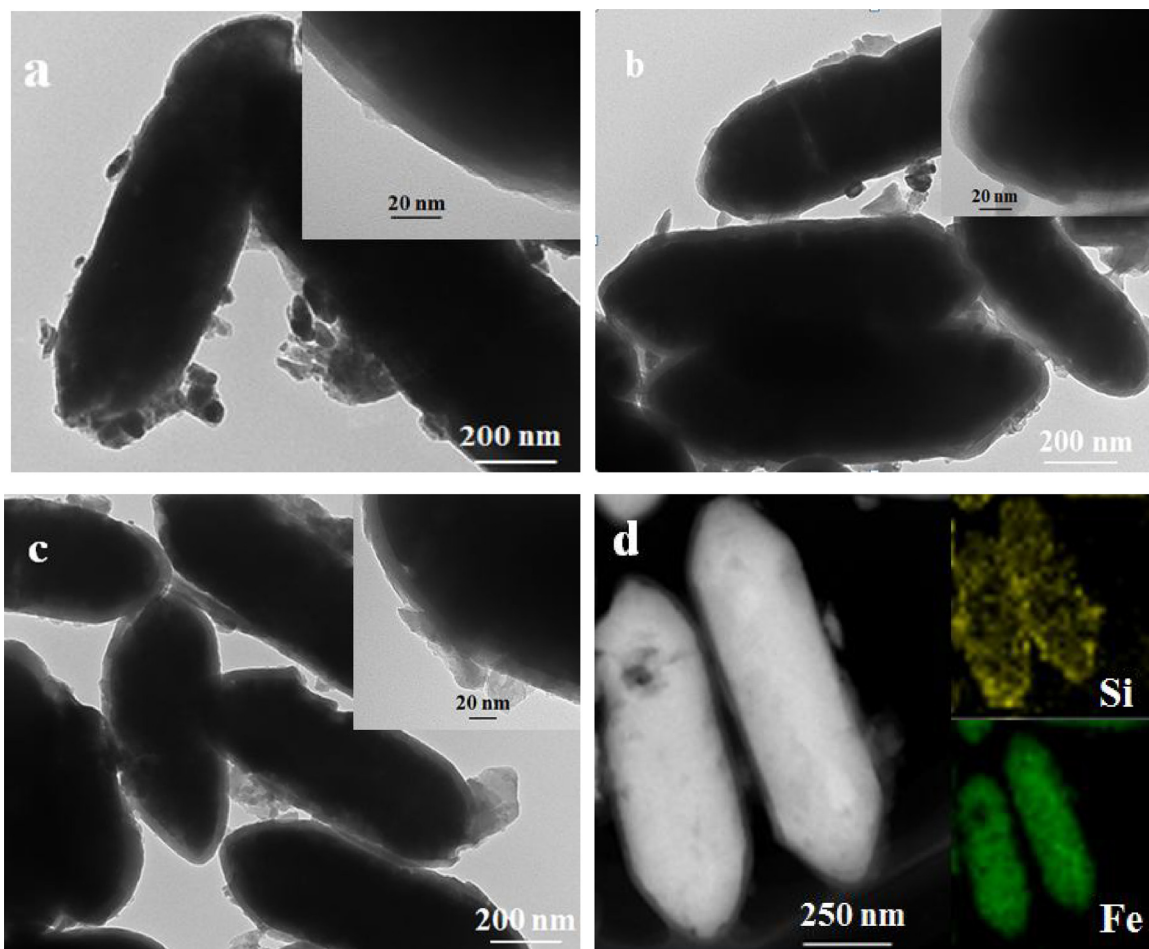


Fig. 3. TEM images of used catalysts for (a) $\text{Fe}_2\text{O}_3@\text{SiO}_2$, (b) $\text{A-Fe}_2\text{O}_3@\text{SiO}_2-(\text{CH}_3)_3$, (c) $\text{B-Fe}_2\text{O}_3@\text{SiO}_2-(\text{CH}_3)_3$ and (d) EDX elemental mapping of $\text{B-Fe}_2\text{O}_3@\text{SiO}_2-(\text{CH}_3)_3$.

Table 1
Textural property of fresh catalyst samples.

Catalyst	BET surface area $A/(\text{m}^2 \text{g}^{-1})$	Pore volume $v/\text{cm}^3 \text{g}^{-1}$	Average pore size d/nm
$\text{Fe}_2\text{O}_3@\text{SiO}_2$	11.61	0.035	11.94
$\text{A-Fe}_2\text{O}_3@\text{SiO}_2-(\text{CH}_3)_3$	12.22	0.068	22.30
$\text{B-Fe}_2\text{O}_3@\text{SiO}_2-(\text{CH}_3)_3$	10.47	0.055	20.90

3. Results and discussion

3.1. Textural properties of the catalysts

The morphology of the synthesized catalyst particles by TEM and SEM characterization are shown in Figs. 2 and S1 for fresh samples and in Fig. 3 for used samples, respectively. As displayed in Fig. 2, $\text{Fe}_2\text{O}_3@\text{SiO}_2$ particles were distinct and complete core-shell structures, similar to those reported in the literature [29]. These particles exhibited good dispersion and had an average length of $1.1 \mu\text{m}$ and a mean width of 360 nm (see Fig. S1a). The thickness of the SiO_2 shell was nearly 15 nm as shown in Fig. 2a. After methyl modification, the shell thickness was increased (see Fig. 2b and 2c). The uniform and smooth SiO_2 shell layer was continuously covered on the surface of Fe_2O_3 nuclear surface, which was proved by EDX mapping analysis of $\text{B-Fe}_2\text{O}_3@\text{SiO}_2-(\text{CH}_3)_3$ (see Fig. 2d) and the other two samples in Fig. S2. The similar morphology displayed in Figs. 2 and S1 indicate that the surface

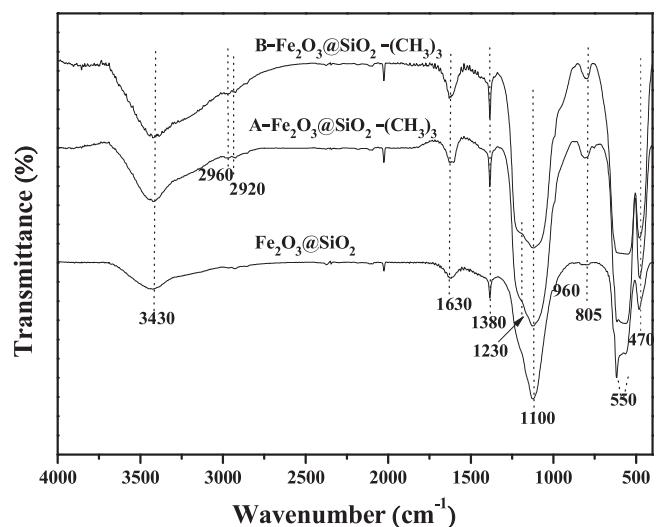


Fig. 4. FT-IR spectra of fresh catalyst samples.

modification does not destroy the core-shell structure of the catalyst. Hence, the SiO_2 shell can be viewed as a vital bridge and ties linking Fe_2O_3 and $-(\text{CH}_3)_3$ that achieves the hydrophobic modification of iron-based catalysts.

For used samples as shown in Fig. 3, it is found that irregular small particles attached to the outer surface of large particles, which may be caused by carbon deposition or heavy hydrocarbon accumulation.

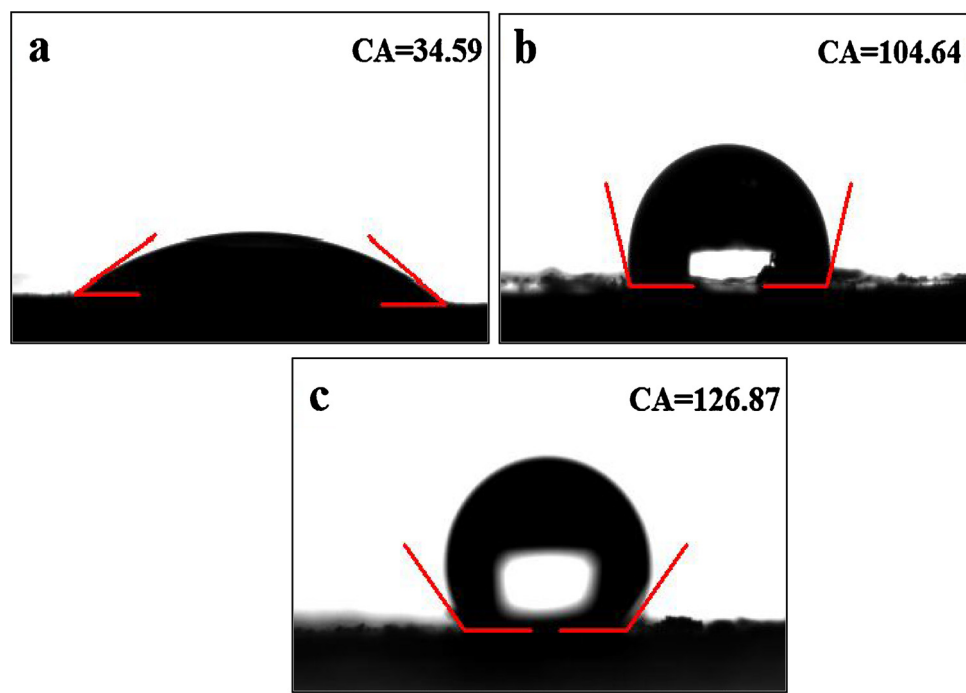


Fig. 5. Water contact angles of (a) $\text{Fe}_2\text{O}_3@\text{SiO}_2$, (b) $\text{A}-\text{Fe}_2\text{O}_3@\text{SiO}_2-(\text{CH}_3)_3$, and (c) $\text{B}-\text{Fe}_2\text{O}_3@\text{SiO}_2-(\text{CH}_3)_3$ samples.

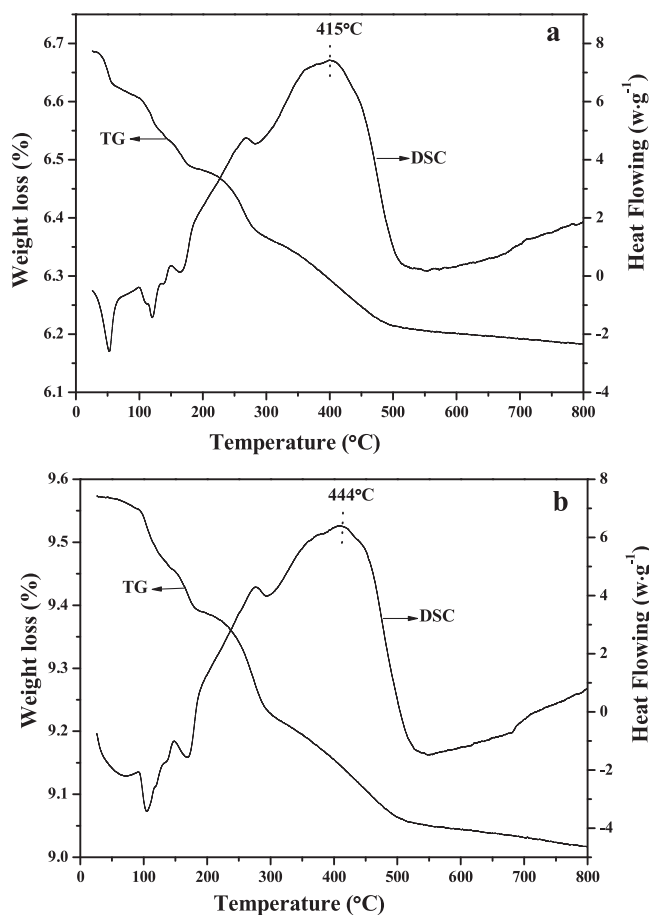


Fig. 6. TG-DSC curves of (a) $\text{A}-\text{Fe}_2\text{O}_3@\text{SiO}_2-(\text{CH}_3)_3$, and (b) $\text{B}-\text{Fe}_2\text{O}_3@\text{SiO}_2-(\text{CH}_3)_3$ samples.

Although the SiO_2 shell became thinner after reaction, the morphology of all used catalyst samples remained and the shell structure was still intact (see Figs. 3 and S3), indicating that the catalysts have good structural stability and then stable activity in FTS.

N_2 adsorption and desorption data are shown in Table 1. $\text{Fe}_2\text{O}_3@\text{SiO}_2$, $\text{A}-\text{Fe}_2\text{O}_3@\text{SiO}_2-(\text{CH}_3)_3$ and $\text{B}-\text{Fe}_2\text{O}_3@\text{SiO}_2-(\text{CH}_3)_3$ showed low BET surface areas. The corresponding pore volume was about 0.035, 0.068, and $0.055 \text{ cm}^3/\text{g}$, respectively. Modification enlarges the pore volume, and average pore size. However, change in the BET surface area was not significant as the level of modification increased. N_2 adsorption isotherms in Fig. S4a shows that three samples had similar pore, belonging to the type III isotherm. The pore-size distribution in Fig. S4b indicates that three samples contained mesopore and macropore. The macropore is likely to be formed by the accumulation of the catalyst particles. This porosity is convenient for the transportation of the products generated during the FTS reaction [29].

3.2. FT-IR analysis of modified $\text{Fe}_2\text{O}_3@\text{SiO}_2$ catalysts

Fig. 4 shows the FT-IR spectra of fresh samples. For all the samples, adsorption peak at 550 cm^{-1} was assigned to Fe-O vibration of Fe_2O_3 [30]. The strong peaks at 1100 cm^{-1} and 470 cm^{-1} were due to Si—O—Si stretching and bending vibration [27,31,32]. The wide band near 3430 cm^{-1} and 1630 cm^{-1} arose from O—H stretching vibration and H—O—H bending vibration of free and adsorbed water [32]. The small peak at 960 cm^{-1} was to the Si—OH stretching vibration [32,33].

For CH_3 modified $\text{A}-\text{Fe}_2\text{O}_3@\text{SiO}_2-(\text{CH}_3)_3$ and $\text{B}-\text{Fe}_2\text{O}_3@\text{SiO}_2-(\text{CH}_3)_3$, there were two new absorption bands at 2960 cm^{-1} and 2920 cm^{-1} , corresponding to symmetric C—H stretches of $-\text{CH}_3$ groups [27]. Absorption peak at 1230 cm^{-1} was symmetric deformation vibration of Si— CH_3 bond [34]. The intensity of the CH_3 bending vibration at 1380 cm^{-1} [27] was increased. Moreover, modified samples had stronger adsorption peak at 805 cm^{-1} caused by Si—C stretching vibration and CH_3 vibration [27]. The peak at 960 cm^{-1} for the Si—OH [35,37] was negligible. These phenomena are attached to the removal of surface terminal polar —OH groups after silylation of SiO_2 surface [37]. For used $\text{A}-\text{Fe}_2\text{O}_3@\text{SiO}_2-(\text{CH}_3)_3$ and $\text{B}-\text{Fe}_2\text{O}_3@\text{SiO}_2-(\text{CH}_3)_3$ (Fig. S5), 2960 cm^{-1} , 2920 cm^{-1} bands for symmetric C—H stretches of $-\text{CH}_3$

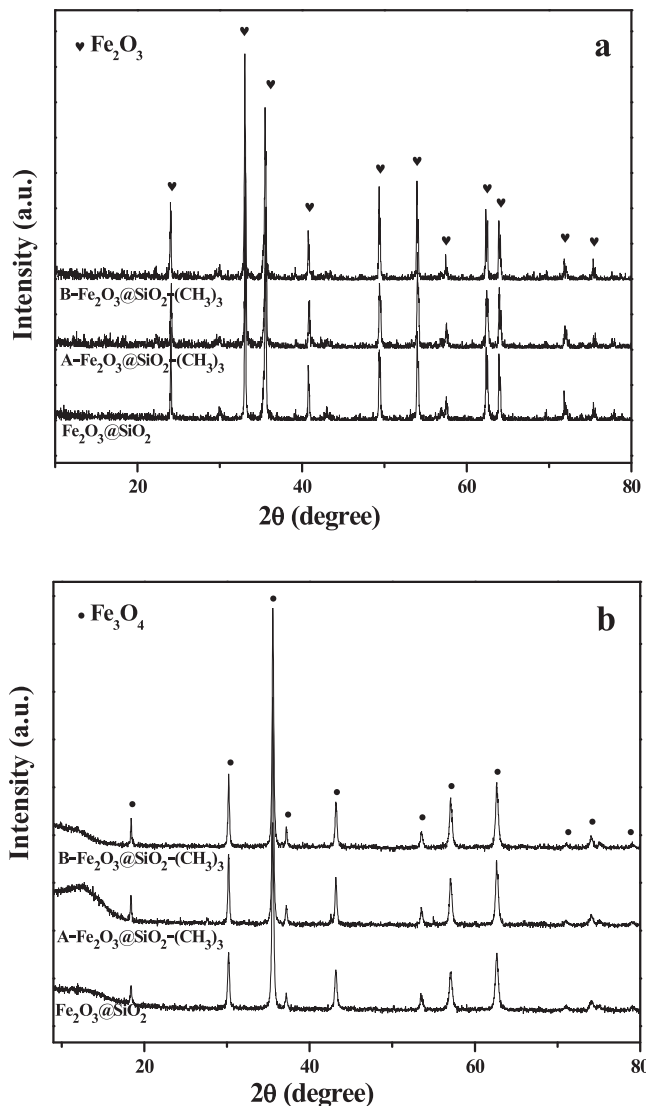


Fig. 7. XRD patterns of fresh (a) and used (b) catalysts.

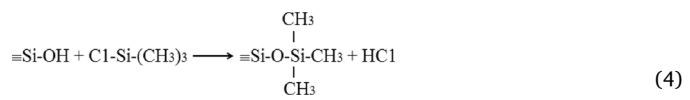
group and 1230 cm^{-1} band for Si–CH₃ bond were still observed. The intensity of the CH₃ vibration peak (1380 cm^{-1}) and Si–C stretching vibration peaks (805 cm^{-1}) decreased slightly, suggesting that the methyl groups are relatively stable under the FTS reaction conditions.

3.3. Contact angle measurement

The hydrophobicity of the samples were characterized further by change of water contact angle as shown in Fig. 5. For unmodified Fe₂O₃@SiO₂ (Fig. 5a), water penetrated into the surface and the contact angle was at 34.59° . For A-Fe₂O₃@SiO₂-(CH₃)₃ and B-Fe₂O₃@SiO₂-(CH₃)₃ (Fig. 5b, 5c), the contact angle became large with increasing TMCS volume, and reached 126.87° for B-Fe₂O₃@SiO₂-(CH₃)₃, indicating an excellent hydrophobicity after surface modification. By means of silylation of silica using TMCS, hydrophobic groups substituting hydrophilic groups has been proved to be one of the effective ways for improving hydrophobicity of SiO₂ surfaces [34–36]. In our experiments, using solvent toluene, the hydrophilic surface (Si-OH groups) of silica becomes hydrophobic by formation of alkoxy-trimethylsilane ($\equiv\text{Si}-\text{O}-\text{Si}(\text{CH}_3)_3$) in certain reaction conditions. In principle, only in the absence of water, TMCS reacts with the hydroxyl groups on the silica surface and can be represented by the following chemical reactions (Eq. (4)):

Table 2
Room temperature ^{57}Fe Mössbauer parameters of the catalysts.

Catalyst	Assignment	Mössbauer parameter			
		IS ^a (mm/s)	QS ^b (mm/s)	H _{hf} ^c (kOe)	Area ^d (%)
Fresh Fe ₂ O ₃ @SiO ₂	Fe ₂ O ₃	0.37	-0.21	518	100
Fresh A-Fe ₂ O ₃ @SiO ₂ -(CH ₃) ₃	Fe ₂ O ₃	0.37	-0.22	517	100
Fresh B-Fe ₂ O ₃ @SiO ₂ -(CH ₃) ₃	Fe ₂ O ₃	0.37	-0.29	517	100
Used Fe ₂ O ₃ @SiO ₂	A-site Fe ₃ O ₄	0.27	-0.01	491	29.42
	B-site Fe ₃ O ₄	0.66		461	58.81
	Fe _x C _y	0.27		217	4.49
		0.20		111	5.50
		0.18		182	1.79
Used A-Fe ₂ O ₃ @SiO ₂ -(CH ₃) ₃	A-site Fe ₃ O ₄	0.16	-0.02	492	30.79
	B-site Fe ₃ O ₄	0.55		461	62.46
	Fe _x C _y	0.27		217	1.27
		0.20		111	4.21
		0.18		182	1.27
Used B-Fe ₂ O ₃ @SiO ₂ -(CH ₃) ₃	A-site Fe ₃ O ₄	0.27	-0.01	492	30.84
	B-site Fe ₃ O ₄	0.66		461	63.07
	Fe _x C _y	0.27		217	0.68
		0.18		182	0.75
		0.20		111	4.66

^a Isomer shift relative to α -Fe.^b Quadrupole splitting.^c Hyperfine field.^d Relative area.

3.4. Thermal stability of modified catalysts

Modified A-Fe₂O₃@SiO₂-(CH₃)₃ (Fig. 6a) exhibited several small endothermic peaks below 200°C corresponding to evaporation of physically adsorbed water and organic components in weight loss of 3.03%. For B-Fe₂O₃@SiO₂-(CH₃)₃ (Fig. 6b), a minor weight loss of 1.95% below 200°C suggests the adsorbed moisture is less. Furthermore, there was a broad exothermic peak at 415°C for A-Fe₂O₃@SiO₂-(CH₃)₃, which means most of the surface Si-CH₃ groups and residual organic groups decompose [26,31,35,38]. For B-Fe₂O₃@SiO₂-(CH₃)₃, a similar exothermic peak at about 444°C , higher than that in A-Fe₂O₃@SiO₂-(CH₃)₃, suggests that surface hydrophobicity improves thermodynamic stability of the catalysts. TG-DSC analysis indicates that modified catalysts of A-Fe₂O₃@SiO₂-(CH₃)₃ and B-Fe₂O₃@SiO₂-(CH₃)₃ are thermally stable below 400°C .

3.5. Phase structure of the catalysts

The structural properties of fresh and used catalysts are shown in Fig. 7. For fresh samples in Fig. 7a, it is revealed that the presence of methyl groups have no effect on the phase structural. All the diffraction patterns were in good agreement with the phase of hematite (α -Fe₂O₃) at 2θ values of 24.2° , 33.1° , 35.6° , 40.8° , 49.5° , 54.0° , 57.6° , 62.5° and 64.0° [15,39]. No peaks of SiO₂ were found, due to the better dispersion of SiO₂, which was uniformly coated on the surface of the hematite (see TEM images in Fig. 2). After CO hydrogenation reaction, the XRD patterns of these catalysts in Fig. 7b exhibited the main characteristic peaks of magnetite (Fe₃O₄) at 2θ values of 30.4° , 35.6° , 43.4° , 57.3° , and 62.9° [40]. No iron carbide in the bulk structure was detected. The bulk phase seems to be stabilized in a highly oxidized state.

It is known that inhibition of water adsorption can prevent iron

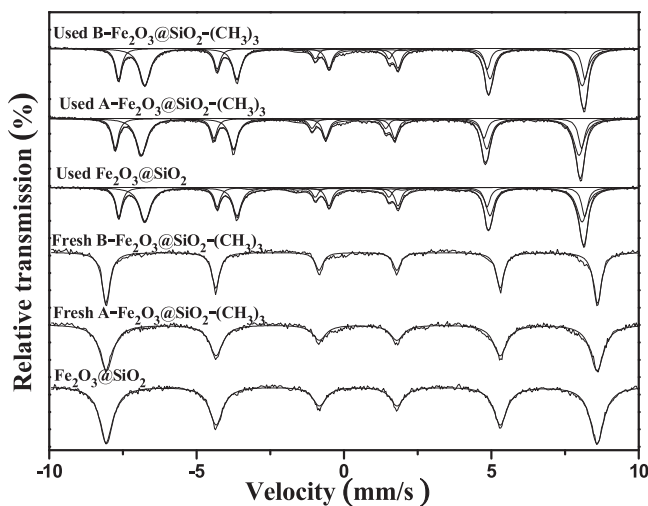


Fig. 8. Mössbauer spectra of fresh and used catalysts.

oxidation during CO hydrogenation [23]. More iron carbides should be detected in used samples in XRD measurement. However, no iron carbides were detected (see Fig. 7b). Therefore, further study by Mössbauer spectroscopy [41,42] was applied to identify all iron species of used catalysts. Table 2 lists the iron-phase composition by fitting the Mössbauer spectra in Fig. 8. The chemical composition of the iron species was mainly in the form of Fe_3O_4 and only a small amount of iron carbides (Fe_xC_y), which is assigned to be Hägg carbide (Fe_5C_2) [41,43]. The content of Fe_xC_y phase in modified catalysts (6.75% and 6.09%, respectively) was slightly lower than that of unmodified $\text{Fe}_2\text{O}_3@\text{SiO}_2$ catalyst (11.78%). It is inferred that the existence of the core-shell structure keeps the catalysts still in an oxidizing environment, and the internal oxidation of the catalyst by water is inevitable. Also, carburization of iron oxides is difficult on larger iron particles. In addition, partial oxidation of used catalyst could happen, when it is exposed to atmosphere during preparation and characterization.

3.6. Reduction behavior of the catalysts

The reduction behavior of hematite can be essentially different depending on the physicochemical characteristics of iron oxides by different preparation methods, the interaction between iron and the presence of additives and reduction conditions. A three-step mechanism $3\text{Fe}_2\text{O}_3 \rightarrow 2\text{Fe}_3\text{O}_4 \rightarrow 6\text{FeO} \rightarrow 6\text{Fe}$ has been proposed for hematite

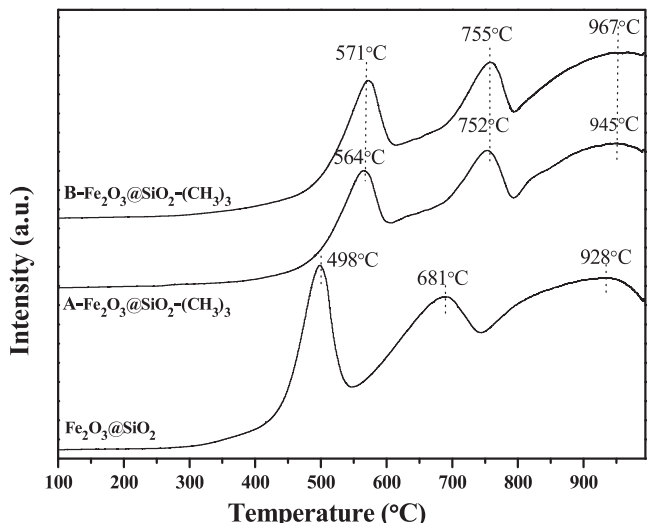
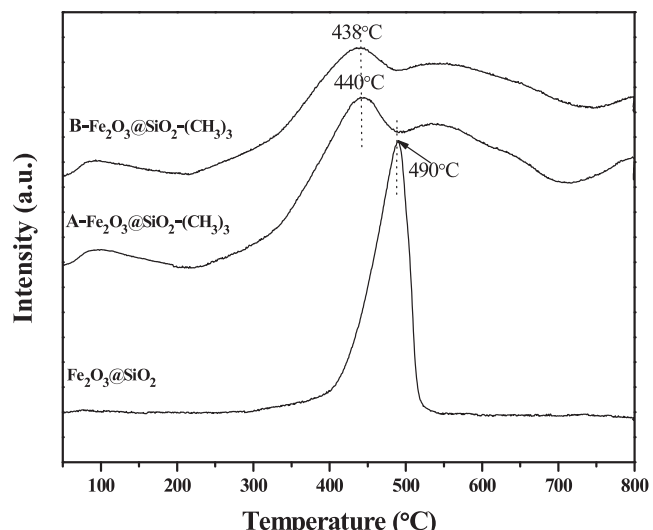
Fig. 9. H_2 -TPR profiles of the catalysts.

Fig. 10. CO-TPD profiles of the catalysts.

reduction [44,45]. As shown in Fig. 9, the TPR profiles of all the samples showed a three-stage reduction, following three-step reduction mechanism. The existence of the core-shell structure makes the reduction of iron difficult compared with the reduction of pure Fe_2O_3 [46,47]. For three samples, the first peak at low temperature is attributed to the reduction of hematite (Fe_2O_3) to magnetite (Fe_3O_4). The middle peak may be attributed to Fe_3O_4 to FeO transformation, whereas the third peak at high temperature is attributed to the reduction of FeO to Fe metal [44]. It can be seen that the whole hydrogen-consuming peaks of CH_3 modified samples shifted to higher temperature, compared with that of $\text{Fe}_2\text{O}_3@\text{SiO}_2$, implying that the reduction of Fe_2O_3 is inhibited after modification.

3.7. CO-TPD measurement of the catalysts

The TPD profiles of pretreated catalyst samples by syngas are shown in Fig. 10. $\text{Fe}_2\text{O}_3@\text{SiO}_2$ appeared a sharp desorption peak at 490 °C, whose shape was similar to the reported [16]. For modified $\text{A-Fe}_2\text{O}_3@\text{SiO}_2-(\text{CH}_3)_3$ and $\text{B-Fe}_2\text{O}_3@\text{SiO}_2-(\text{CH}_3)_3$ samples, two broad peaks can be distinguished in the temperature range of 350 °C–690 °C. The desorption temperature at around 440 °C was lower than that of $\text{Fe}_2\text{O}_3@\text{SiO}_2$, suggesting that surface modification slightly weakens the adsorption strength. The higher temperature broad desorption peak at about 540 °C was ascribed to the desorption of CO adsorbed dissociatively and recombined to desorb on the surface [29,48]. Surface modification did not reduce the adsorption amount of CO, according to the entire peak areas for three samples.

3.8. XPS measurement of the catalysts

As shown in Table 3, surface Fe content for the used samples was increased compared with that of the fresh samples, which was ascribed to decrease in film thickness of SiO_2 (Fig. 3). However, the Fe/Si ratio showed that the surface was still covered with a large amount of Si after reaction, further proving that the core-shell structure is highly stable during CO hydrogenation. Surface carbon deposition was increased significantly after reaction. The XPS spectra of Fe (2p) and C (1s) for the fresh and used samples are shown in Fig. S6. The intensity of Fe (2p) spectrum (Fig. S6a) was greatly attenuated by the coverage of SiO_2 layer for both fresh and used samples (see Figs. 2 and 3). The binding energy (B.E.) of the Fe (2p3/2) peak at 711.9 eV and Fe (2p1/2) at around 725.2 eV was attributed to the existence of Fe_2O_3 for fresh samples, and peaks of Fe_3O_4 in the range of $\text{Fe}2\text{p}3/2$ (710.6 eV) and $\text{Fe}2\text{p}1/2$ (724.5 eV) for used samples. The B.E. of Fe 2p was higher than

Table 3
Surface composition (at. %) of fresh and used catalysts.

Catalyst	Atomic (%)				Atomic ratio
	C1s	Fe2p	Si2p	O1s	
	Fe/Si				
Fe ₂ O ₃ @SiO ₂ ^a	29.42	0.22	25.22	45.13	0.01
A-Fe ₂ O ₃ @SiO ₂ -(CH ₃) ₃ ^a	18.72	0.86	30.59	49.82	0.03
B-Fe ₂ O ₃ @SiO ₂ -(CH ₃) ₃ ^a	17.13	0.97	31.33	50.57	0.03
Fe ₂ O ₃ @SiO ₂ ^b	43.30	2.45	16.95	37.30	0.14
A-Fe ₂ O ₃ @SiO ₂ -(CH ₃) ₃ ^b	33.69	1.89	21.45	42.97	0.09
B-Fe ₂ O ₃ @SiO ₂ -(CH ₃) ₃ ^b	39.89	1.76	19.26	39.08	0.09

^a Fresh samples.

^b Used samples.

that reported data [16,49], which is due to the strong interaction between iron and silicon [41]. No carbide carbon was observed.

3.9. Catalytic performance

Effects of surface modification of the catalysts on the activity and product distribution of FTS are shown in Fig. 11. Fe₂O₃@SiO₂ exhibited the highest activity with an average CO conversion of 96%, while with lower selectivity of light olefins (C₂=C₄= fraction) and higher CH₄ content (Fig. 11a). Modified catalysts displayed lower activity but better hydrocarbon distribution, which produced more olefin products and less CH₄ in hydrocarbon distribution. The CO conversion remained almost constant over 120 h on stream (see Fig. S7) as the catalyst had good structural stability (Fig. 3). Most importantly, great decrease in the CO₂ selectivity was found over modified catalysts (Fig. 11c and 11d), compared with over Fe₂O₃@SiO₂ catalyst (Fig. 11b). Calculated space time yield over Fe₂O₃@SiO₂, A-Fe₂O₃@SiO₂-(CH₃)₃, and B-Fe₂O₃@SiO₂-(CH₃)₃ were 6.71×10^{-6} mol_{CO} g_{cat}⁻¹ s⁻¹, 4.64×10^{-6} mol_{CO} g_{cat}⁻¹ s⁻¹, and 4.20×10^{-6} mol_{CO} g_{cat}⁻¹ s⁻¹, respectively. It is known that inhibition of water readsorption can accelerate the rate of FTS [23]. Also, surface modification does not reduce the adsorption amount of CO as shown Fig. 10. However, decreasing trend in the activity suggests that the real reaction process is quite different from the adsorption environment operated in CO-TPD measurement. Significant decrease in activity on modified is deduced due mainly to the change in hydrocarbons adsorption and the influence of steric hindrance. Since the modification shows great influence on the adsorption of water, the redsorption and desorption behavior of hydrocarbons may also change after modification, which will affect the adsorption behavior of CO and H₂ and the reactivity. Moreover, tri-methyl can form a hydrophobic umbrella structure [36] that has a great steric hindrance [27], resulting in a decrease in the active site number exposed to the catalyst surface or inhibition of the rapid diffusion of the initial hydrocarbon products. Further decrease in activity was observed as the increase of TMCS content.

In FTS water is produced in large quantities on iron-based catalyst. High partial pressure of H₂O produced will accelerate the WGS reaction [11]. XRD (Fig. 7b) and Mössbauer spectroscopy (Fig. 8) analysis show that for the three used catalysts, the bulk phase is stabilized in the form of Fe₃O₄, the most active phase for WGS reaction among the iron-containing phases formed during FTS [24]. The WGS activity should be high over Fe₃O₄. However, CO₂ is greatly reduced over modified catalysts. Thus it can be seen that surface modification has played an important role in preventing the readsorption of water to reduce CO₂ generation from about 40% to less than 5% in carbon basis (see Fig. 11b-d). Trimethylchlorosilane as a hydrophobic modifier, can connect SiO₂ and Si-(CH₃)₃ on the catalyst surface to form a hydrophobic membrane [36], endowing the catalyst a strong hydrophobic capacity to prevent readsorption of water. The generated water will leave the catalyst surface timely [27]. Inhibition of water readsorption thereby reduces the activity of the WGS reaction. Calculated outlet H₂/CO molar ratio was significantly decreased from 32.2 on Fe₂O₃@SiO₂ to

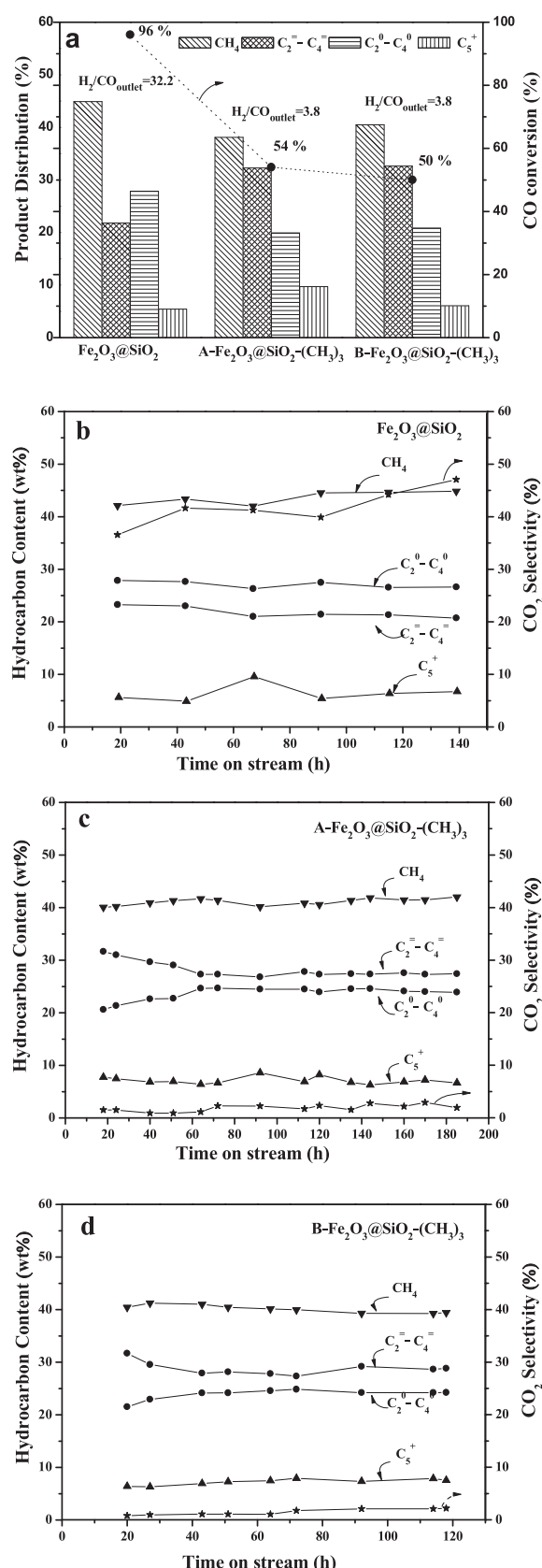


Fig. 11. Activity and product distribution of (a) and stability of Fe₂O₃@SiO₂ (b), A-Fe₂O₃@SiO₂-(CH₃)₃ (c), and B-Fe₂O₃@SiO₂-(CH₃)₃ (d) with time on stream.
Reaction conditions: H₂/CO = 2, 3000 h⁻¹, 320 °C, 1.5 MPa.

3.8 on two modified catalysts, providing direct evidence of the inhibition of WGS reaction (see Fig. 11a).

It is reported that catalytic active sites for the undesired side reactions can be poisoned or covered by forming the core shell structure to achieve high selectivity [50]. High selectivity can also be attained by regulating the diffusion rates of both reactants and products on the active sites through tuning the shell porosity, pore size, shell hydrophobicity and shell thickness [51]. In this work, we found that the core-shell catalyst has a certain morphological advantages. The active sites for FTS were surrounded by a hydrophobic shell to form a fully hydrophobic environment, which can effectively inhibit the readsorption of water and thus the WGS reaction.

High WGS reaction activity is often associated with higher surface H₂/CO ratio adsorbed on the catalyst surface, favoring chain termination reactions and results in high amount of CH₄ and low molecular saturated hydrocarbons [20,23]. On the contrary, the inhibition of WGS reaction will reduce hydrogenation ability of the catalyst to produce more olefin products [52], as illustrated in Fig. 11a. For FTS, high partial pressure of water is a main cause of deactivation and inhibits the rate of FTS for hydrocarbon production. The hydrophobic surface is favorable to reduce the production of CO₂ and improve the stability of the catalysts by preventing the readsorption of water and suppressing the WGS reaction in this experiment. However, the influence on hydrocarbon adsorption is still not clear. These phenomena need to be further studied.

4. Conclusions

A novel hydrophobic modified core-shell Fe₂O₃@SiO₂-(CH₃)₃ catalyst with the SiO₂ shell bridge between Fe₂O₃ and -(CH₃)₃ was synthesized to explore the influence of the hydrophobicity on the catalytic performance for the FTS reaction. During CO hydrogenation, the core-shell structure remains to obtain high activity and stability. Hydrophobic modification greatly reduces the selectivity of CO₂ by suppressing the WGS activity. The selectivity of light olefin is increased by adjusting the H₂/CO molar ratio to weaken the hydrogenation capacity in the real reaction. This study provides a method for tuning the product distribution by changing the hydrophobic properties of the catalyst, in particular for FTS reaction where water is generated and reparticipates in the reaction.

Acknowledgments

Financial supports from the National Natural Science Foundation of China (Nos. 21666030, 21366025), the National First-rate Discipline Construction Project of Ningxia (Chemical Engineering & Technology, NXYLXK2017A04) and the Foundation of State Key Laboratory for Physical Chemistry of Solid Surfaces in Xiamen University (201623) are greatly acknowledged.

Appendix A. Supplementary data

Supplementary material related to this article can be found, in the online version, at doi:<https://doi.org/10.1016/j.apcatb.2018.03.048>.

References

- [1] K. Cheng, W. Zhou, J.C. Kang, S. He, S.L. Shi, Q.H. Zhang, Y. Pan, W. Wen, Y. Wang, *Chemistry* 3 (2017) 334.
- [2] Q.H. Zhang, J.C. Kang, Y. Wang, *ChemCatChem* 2 (2010) 1030.
- [3] B. Zhao, P. Zhai, P.F. Wang, J.Q. Li, T. Li, M. Peng, M. Zhao, G. Hu, Y. Yang, Y.W. Li, Q.W. Zhang, W.B. Fan, D. Ma, *Chemistry* 3 (2017) 323.
- [4] J.C. Kang, K. Cheng, L. Zhang, Q.H. Zhang, J.S. Ding, W.Q. Hua, Y.C. Lou, Q.G. Zhai, Y. Wang, *Angew. Chem. Int. Ed.* 50 (2011) 5200.
- [5] J. Bao, J.J. He, Y. Zhang, Y. Yoneyama, N. Tsubaki, *Angew. Chem. Int. Ed.* 47 (2008) 353.
- [6] H.M.T. Galvis, J.H. Bitter, C.B. Khare, M. Ruitenbeek, A.I. Dugulan, K.P. de Jong, *Science* 335 (2012) 835.
- [7] F. Jiao, J.J. Li, X.L. Pan, J.P. Xiao, H.B. Li, H. Ma, M.M. Wei, Y. Pan, Z.Y. Zhou, M.R. Li, S. Miao, J. Li, Y.F. Zhu, D. Xiao, T. He, J.H. Yang, F. Qi, Q. Fu, X.H. Bao, *Science* 351 (2016) 1065.
- [8] K. Cheng, B. Gu, X.L. Liu, J.C. Kang, Q.H. Zhang, Y. Wang, *Angew. Chem. Int. Ed.* 55 (2016) 4725.
- [9] L.S. Zhong, F. Yu, Y.L. An, Y.H. Zhao, Y.H. Sun, Z.J. Li, T.J. Lin, Y.J. Lin, X.Z. Qi, Y.Y. Dai, L. Gu, J.S. Hu, S.F. Jin, Q. Shen, H. Wang, *Nat. Chem.* 538 (2016) 84.
- [10] Y.L. Zhang, L.L. Ma, T.J. Wang, X.J. Li, *Fuel* 177 (2016) 197.
- [11] Z.H. Li, R.J. Liu, Y. Xu, X.B. Ma, *Appl. Surf. Sci.* 347 (2015) 643.
- [12] C.G. Visconti, M. Martinelli, L. Falbo, A. Infantes-Molina, L. Lietti, P. Forzatti, G. Iaquaniello, E. Palo, B. Picutti, F. Brignoli, *Appl. Catal. B: Environ.* 200 (2017) 530.
- [13] S. Li, S. Krishnamoorthy, A. Li, G.D. Meitzner, E. Iglesia, *J. Catal.* 206 (2002) 202.
- [14] R.A. Dector, A.T. Bell, *J. Catal.* 97 (1986) 121.
- [15] Y. Yang, H.W. Xiang, Y.Y. Xu, L. Bai, Y.W. Li, *Appl. Catal. A* 266 (2004) 181.
- [16] J.L. Zhang, L.H. Ma, S.B. Fan, T.S. Zhao, Y.H. Sun, *Fuel* 109 (2013) 116.
- [17] S. Lögdberg, D. Tristantini, Ö. Borg, L. Ilver, B. Gevert, S. Järås, E.A. Blekkan, A. Holmen, *Appl. Catal. B: Environ.* 89 (2009) 167.
- [18] O.O. James, B. Chowdhury, M.A. Mesubi, S. Maiti, *RSC Adv.* 2 (2012) 7347.
- [19] L.M. Chew, P. Kangavansura, H. Ruland, H.J. Schulte, C. Somsen, W. Xia, G. Eggeler, A. Worayingyong, M. Muhler, *Appl. Catal. A* 482 (2014) 163.
- [20] Y. Liu, C.H. Zhang, Y. Wang, Y. Li, X. Hao, L. Bai, H.W. Xiang, Y.Y. Xu, B. Zhong, Y.W. Li, *Fuel Process. Technol.* 89 (2008) 234.
- [21] C.M. Li, I. Sayaka, F. Chisato, K. Fujimoto, *Appl. Catal. A* 509 (2016) 123.
- [22] Y. Liu, B.T. Teng, X.H. Guo, Y. Li, J. Chang, L. Tian, X. Hao, Y. Wang, H.W. Xiang, Y.Y. Xu, Y.W. Li, *J. Mol. Catal. A Chem.* 272 (2007) 182.
- [23] D.B. Bukur, B. Todic, N. Elbashir, *Catal. Today* 275 (2016) 66.
- [24] Y. Cheng, J. Lin, T.J. Wu, H. Wang, S.H. Xie, Y. Pei, S.R. Yan, M.H. Qiao, B.N. Zong, *Appl. Catal. B: Environ.* 204 (2017) 475.
- [25] E. Ryttner, A.R. Salman, N.E. Tsakounis, R. Myrstad, J. Yang, S. Lögdberg, A. Holmen, M. Rønning, *Catal. Today* 299 (2018) 20.
- [26] L.H. Shi, J.G. Chen, K.G. Fang, Y.H. Sun, *Fuel* 87 (2008) 521.
- [27] L.H. Shi, D.B. Li, B. Hou, Y.H. Sun, *Chin. J. Catal.* 28 (2007) 999.
- [28] L.H. Jia, L.T. Jia, D.B. Li, B. Hou, J.G. Wang, Y.H. Sun, *J. Solid State Chem.* 184 (2011) 488.
- [29] Y.L. Zhang, T.J. Wang, L.L. Ma, N. Shi, D.F. Zhou, X.J. Li, *J. Catal.* 350 (2017) 41.
- [30] S.M. Rodolfo-Baechler, S.L. González-Cortés, J. Orozco, V. Sagredo, B. Fontal, A.J. Mora, G. Delgado, *Mater. Lett.* 58 (2004) 2447.
- [31] J.L. Gurav, A.V. Rao, U.K.H. Bangi, *J. Alloys Compd.* 471 (2009) 296.
- [32] H.J. Liu, W. Sha, A.T. Cooper, M. Fan, *Colloids Surf. A: Physicochem. Eng. Aspects* 347 (2009) 38.
- [33] J.J. Li, J.G. Cao, L. Huo, X.D. He, *Mater. Lett.* 87 (2012) 146.
- [34] R. Al-Oweini, H. El-Rassy, *J. Mol. Struct.* 919 (2009) 140.
- [35] S. He, D.M. Huang, H.J. Bi, Z. Li, H. Yang, X.D. Cheng, *J. Non-Cryst. Solids* 410 (2015) 58.
- [36] W.Z. Zheng, W.G. Ding, B.J. Ouyang, H.J. Chen, Z.Y. Chi, *Adv. Mater. Res.* 163 (2011) 770.
- [37] M. Li, H.Y. Jiang, D. Xu, O. Hai, W. Zheng, *J. Non-Cryst. Solids* 452 (2016) 187.
- [38] A.V. Rao, S.S. Latthe, S.L. Dhere, S.S. Pawar, H. Imai, V. Ganeshan, S.C. Gupta, P.B. Wagh, *Appl. Surf. Sci.* 256 (2010) 2115.
- [39] S.H. Kang, J.W. Bae, P.S.S. Prasad, S.J. Park, K.J. Woo, K.W. Jun, *Catal. Lett.* 130 (2009) 630.
- [40] S. Özkar-Aydinoğlu, Ö. Atac, Ö.F. Güll, S. Kinayiğit, S. Sal, M. Baranak, İ. Boz, *Chem. Eng. J.* 181 (2012) 581.
- [41] J. Xu, C.H. Bartholomew, *J. Phys. Chem. B* 109 (2005) 2392.
- [42] X.N. Li, K.Y. Zhu, J.F. Pang, M. Tian, J.Y. Liu, A.I. Rykov, M.Y. Zheng, X.D. Wang, X.F. Zhu, Y.Q. Huang, B. Liu, J.H. Wang, W.S. Yang, T. Zhang, *Appl. Catal. B: Environ.* 224 (2018) 518.
- [43] N. Sirimanathan, H.H. Hamdeh, Y.Q. Zhang, B.H. Davis, *Catal. Lett.* 82 (2002) 181.
- [44] G. Kishan, M.W. Lee, S.S. Nam, M.J. Choi, K.W. Lee, *Catal. Lett.* 56 (1998) 215.
- [45] W.K. Jozwiak, E. Kaczmarek, T.P. Maniecki, W. Ignaczak, W. Manukiewicz, *Appl. Catal. A: Gen.* 326 (2007) 17.
- [46] N. Chen, J.L. Zhang, Q.X. Ma, S.B. Fan, T.S. Zhao, *RSC Adv.* 6 (2016) 34204.
- [47] A.J. Ma, S.Z. Wang, C. Liu, H. Xian, Q. Ding, L. Guo, M. Meng, Y.S. Tan, N. Tsubaki, J. Zhang, L.R. Zheng, X.G. Lia, *Appl. Catal. B: Environ.* 146 (2014) 24.
- [48] P. Sharma, T. Elder, L.H. Groom, J.J. Spivey, *Top. Catal.* 57 (2014) 526.
- [49] J.P. Baltrus, J.R. Diehl, M.A. McDonald, M.F. Zarochak, *Appl. Catal. A* 48 (1989) 199.
- [50] P.P. Zhang, L. Tan, G.H. Yang, N. Tsubaki, *Chem. Sci.* 8 (2017) 7941.
- [51] Z.W. Li, M. Li, Z.F. Bian, Y. Kathiraser, S. Kawi, *Appl. Catal. B: Environ.* 188 (2016) 324.
- [52] J.L. Zhang, K.G. Fang, K. Zhang, W.H. Li, Y.H. Sun, *Korean J. Chem. Eng.* 26 (2009) 890.